Extraordinary transmission without resonance: Probing enhancements in acoustic transmission and energy density in hole arrays acting as a metasurface

E. Bok,[1,*] J. J. Park,[2] A. A. Maznev,[3] S. H. Lee,[2] and O. B. Wright[4,5,†]

[1]*Division of Applied Physics, Faculty of Engineering, Hokkaido University, Sapporo 060-8628, Japan*
[2]*Institute of Physics and Applied Physics, Yonsei University, Seoul 03722, Korea*
[3]*Department of Chemistry, Massachusetts Institute of Technology, Cambridge, Massachusetts 02139, USA*
[4]*Hokkaido University, Sapporo 060-0808, Japan*
[5]*Graduate School of Engineering, Osaka University, Yamadaoka 2-1, Suita, Osaka 565-0871, Japan*

(Received 20 July 2022; revised 21 June 2023; accepted 31 August 2023; published 30 October 2023)

Extraordinary transmission in wave physics, such as in optics or acoustics, is related to the theory of metamaterials in which resonances enhance wave transmission through apertures. Near-perfect acoustic transmission can, however, exist for subwavelength apertures in a thin wall without resonance, strongly contrasting to the situation in optics. We demonstrate this by experiments on airborne acoustic transmission through metal plates perforated with a variable number of circular holes at constant filling fraction $\alpha \sim 0.12$ in a waveguide. Dissipative theory, including interactions between holes, shows that, at near-unity transmittance, the holes act as a low-inertance metasurface, which is verified by simulations. We also present a simple equation for the lossless, thin-wall case. Calculated enhancements in power transmission and acoustic energy density, which agree with the maximum measured values $\sim$7 and 27 for constant α, are close to the lossless values $1/\alpha$ and $1/(2\alpha^2)$, respectively, and are also close to simulations, obtained at 1 kHz for one hundred 3.5 mm diameter holes in a 1 mm thick wall. Conditions for the maximum transmission enhancement in the general case are also obtained, demonstrating the counterintuitive result that the enhancement is optimal at $\sim$50% power transmission.

DOI: 10.1103/PhysRevB.108.144111

I. INTRODUCTION

The transmission of waves through small subwavelength holes in an opaque screen is a classic problem in optics and acoustics [1–5]. The effect can be quantified by the transmission efficiency η, i.e., the ratio of the total transmitted power to the incident power on the open hole area [2–6]. Extraordinary transmission, i.e., for which $\eta > 1$, has attracted significant attention in the context of recent metamaterials research, allowing the super-concentration of energy in regions much smaller than the wavelength λ with subwavelength optical [6–8] or acoustic [9–23] resonators, sometimes involving bare holes. In particular, in acoustics, extraordinary transmission has been demonstrated for sound in fluids [9–14,16–21] and solids [15,22,23]. In both optics and acoustics, all these methods rely on resonances, which underpin the response of metamaterials. In acoustics, these can be Fabry-Pérot resonances in apertures, surface-wave resonances in grooves near apertures, membrane resonances, or cavity resonances, for example.

Although resonances are essential in optics to overcome poor transmission through bare holes [6–8], this is not so in fluid acoustics [3,24–30]: at low frequencies, a plate perforated with bare holes can transmit nearly all the sound normally incident on it, which has practical applications in sound transparent screens [31,32]. Equivalently, it suffices for a given aperture filling fraction α to overcome poor transmission by simply reducing the hole radius $r \ll \lambda$, provided that the apertures are contained in a wall of thickness $w \ll \lambda$. Low-frequency perfect transmission in a multihole array is a well-known phenomenon in acoustics. However, it has not been systematically interpreted in terms of extraordinary transmission. With such a viewpoint, one can ascertain that low-frequency extraordinary transmission with $\eta > 1$ was clearly observed in previous works [27,29,31,32]. Phong *et al.*, for example, demonstrated extraordinary transmission with $\eta \approx 5$ and α down to $\sim$0.2 [29], whereas Mulholland and Parbrook achieved a similar η with $\alpha \sim 0.005$ [27]. Although such nonresonant enhancements in transmission efficiency could potentially be an excellent strategy for wideband efficient energy harvesting, a detailed analysis of the acoustic extraordinary transmission, in particular its optimization, has been lacking. Moreover, such phenomena have not been analyzed in the context of metamaterial physics, which gives a more intuitive insight into the mechanisms involved.

Here we reexamine the resonance-free enhancement in acoustic transmission through bare holes, together with the accompanying energy concentration, in terms of extraordinary transmission of a metasurface, and elucidate the factors that limit the maximum transmission efficiency. Furthermore, we suggest more precise expressions for the metamaterial-based model of the transmission than those introduced in previous work [18], including the effect of interactions between holes which is vital for accurate predictions, and verify our

*eunbok81@gmail.com
†olly@eng.hokudai.ac.jp

calculations using a theory based on far-field waves and the use of boundary conditions that replace the effect of viscous losses and interactions in the acoustic near field, as well as by numerical simulation. We conduct experiments in an air-filled tube containing plates with different numbers of holes at constant filling fraction—a rarely used experimental approach [31]—recording transmission efficiencies up to ∼7 and an acoustic energy densification ∼30.

II. METASURFACE THEORY OF ACOUSTIC TRANSMISSION THROUGH HOLES

To analyze the transmission through a hole array, consider a rigid wall of thickness w perforated with N identical circular holes of radius r placed in a circular waveguide of diameter D, under the assumptions $w, r, D \ll \lambda$, where λ is the acoustic wavelength and $\alpha = N\pi r^2/S = 4r^2N/D^2 \ll 1$ is the hole filling fraction, where $S = \pi D^2/4$. The case $N = 1$ is included in this analysis. We consider the air plug in a hole to be accelerated by the acoustic pressure difference across it owing to plane-wavefront incidence. This lumped element approach for metasurfaces was taken previously [18], but we extend it to include the near-field acoustic interaction between holes [48]. The response to sinusoidal variations at angular frequency ω, $\propto \exp(-i\omega t)$, is dictated by an equation depending on the effective mass M_{eff} and damping coefficient b of each hole in the form [18]

$$(p_1 - p_2)\pi r^2 = M_{\text{eff}}\ddot{\xi} + b\dot{\xi} = (-i\omega M_{\text{eff}} + b)\dot{\xi}, \quad (1)$$

where p_1 and p_2 are the complex acoustic pressures just before and after the wall, and $\dot{\xi}$ is the axial air-plug velocity.

Analytical expressions can be derived as follows, as shown in detail in the Supplemental Material [49]

$$M_{\text{eff}} = \pi r^2 w' \rho_0 \left(1 + \frac{w''}{w'}\frac{\delta}{r}\right), \quad (2)$$

$$b = \pi r w'' \rho_0 \omega \delta, \quad (3)$$

where skin depth $\delta = \sqrt{2\mu/\omega\rho_0}$ (assumed $\ll \sqrt{2}r$) [33], and ρ_0 and μ are the density and dynamic viscosity of air. The effective lengths $w' = w + 2\Delta w$, where $\Delta w = 8\psi(\sqrt{\alpha})r/3\pi$, and $w'' = w + 2r$, approximate forms introduced respectively in Refs. [28] and [26], are related to the acoustic inertance (i.e., an inductivelike acoustic response) and the acoustic resistance, respectively, the former being dependent on the Fok function [28,34–36] $\psi(y)$ [50]— which accounts for the near-field interactions between the deeply subwavelength separated holes or with the waveguide walls—and the latter on the fluid flow distortion in the vicinity of each hole. This treatment also applies for $N = 1$ owing to the interaction with the waveguide wall [29]. The Fok-function dependent normalized end correction $\Delta w/r$, for example, takes the values 0.73, 0.48, and 0.11 for filling fraction $\alpha = 0.01$, 0.1, and 0.5, respectively.

The acoustic pressure fields, related to the amplitude reflection and transmission coefficients R and T, are $p_1 = p_1^+(1 + R)$ and $p_2 = p_1^+T$, where p_1^+, p_1^+R, and p_1^+T are the complex incident, reflected, and transmitted waves. The normal particle velocities just before and after the perforated wall are $u_1 = p_1^+(1 - R)/\rho_0 c_0$, where c_0 is the sound velocity, and $u_2 = p_1^+T/\rho_0 c_0$. Mass flux continuity [37] for a lumped air plug implies $\dot{\xi} = u_2/\alpha$ and $u_1 = u_2$, so Eq. (1) leads to

$$1 - \frac{1+R}{T} = \frac{i\omega M_{\text{eff}} - b}{\pi r^2 \alpha \rho_0 c_0}, \quad (4)$$

$$T = \frac{1}{1 + \frac{b - i\omega M_{\text{eff}}}{2\pi r^2 \alpha \rho_0 c_0}}, \quad (5)$$

where $1 - R = T$, in agreement with the equations of Park *et al.* [18]. Substituting for M_{eff} and b from Eqs. (2) and (3) and assuming $\delta/r \ll 1$, the power transmission and reflection coefficients, $\tau = |T|^2$ and $\Gamma = |R|^2$, can be expressed in the form

$$\tau = \frac{1}{1+\chi^2}\left[1 - 2\frac{\delta}{r}\frac{w''}{w'}\frac{(1+\chi)\chi}{1+\chi^2}\right], \quad (6)$$

$$\Gamma = \frac{\chi^2}{1+\chi^2}\left[1 + 2\frac{\delta}{r}\frac{w''}{w'}\frac{1-\chi}{1+\chi^2}\right], \quad (7)$$

similar to the equations in Refs. [38] and [39] (see the Supplemental Material [49]), where $\chi = kw'/2\alpha$ and $k = \omega/c_0$ is the wave number. The absorption coefficient is $A = 1 - (\tau + \Gamma)$. This metamaterial-based model is a leading-order approximation for $\alpha \ll 1$ and $kw \ll 1$ of a more precise model (see the Supplemental Material) based on far-field waves and the use of boundary conditions that replace the effect of viscous losses and interactions in the acoustic near field.

It is instructive to consider the lossless case, $b = 0$, in the limit of N sparsely arranged holes ($\alpha \to 0$), so that Fok-function related near-field interactions can be neglected. Equation (6) then reduces to

$$\tau = \frac{1}{1 + \frac{1}{4}\left(\frac{\omega M_{\text{eff}}}{\pi r^2 \alpha \rho_0 c_0}\right)^2} = \frac{1}{1 + \frac{1}{4}\left(\frac{kw}{\alpha}\right)^2\left(1 + \frac{2\Delta w}{w}\right)^2}, \quad (8)$$

where $\Delta w = (8/3\pi)r \approx 0.85r$ is the conventional Rayleigh end correction [3,37]. For a variable number of holes N, consider decreasing their radius from an initial value $r \gg w$ while keeping the filling fraction α and thickness w constant. While $r \gg w$, Eq. (8) reduces to

$$\tau = \frac{1}{1 + \left(\frac{8}{3\pi}\right)^2\left(\frac{kr}{\alpha}\right)^2}. \quad (9)$$

In this thin wall, lossless regime one obtains a higher τ by increasing N (i.e., decreasing r). Also, in this regime, $\tau = 1$ if $r \to 0$, which is quite a startling result.

This counterintuitive behavior—transmission increasing with decreasing hole size at constant filling fraction α and thickness w—is regulated by the corresponding decrease in the end correction $\Delta w(r)$ in Eq. (8). To understand this, consider the wall of holes as a metasurface characterized by the acoustic inertance I_{eff} [37]—the equivalent of inertia for sound waves—which is a measure of the pressure difference Δp required to cause a unit change in the rate of change of volumetric flowrate Q with time $I_{\text{eff}} \equiv \Delta p/\dot{Q} = i(p_1 - p_2)/(\omega S u_2)$.

To see how I_{eff} affects τ, consider the lossless case. Substituting $\dot{\xi} = u_2/\alpha$ into Eq. (1) with damping coefficient $b = 0$ yields $I_{\text{eff}} = M_{\text{eff}}/N(\pi r^2)^2$. I_{eff} can be quantified by the dimensionless variable $\omega I_{\text{eff}}/Z_g$, where $Z_g = \rho_0 c_0/S$ is the waveguide acoustic impedance. Equa-

tion (8) for this lossless case predicts near-unity transmission when $\omega M_{\text{eff}}/(\pi r^2 \alpha \rho_0 c_0) = \omega I_{\text{eff}}/Z_g = (kw/\alpha)(1 + 2\Delta w/w) \ll 1$. In other words, when $\tau \approx 1$ the collection of holes approaches the behavior of a low-inertance metasurface. By means of Eq. (2) and the relation $u_2 = p_2/\rho_0 c_0$, this translates as $\omega I_{\text{eff}}/Z_g = i(p_1 - p_2)/p_2 \ll 1$, i.e., $p_1 \approx p_2$ in Eq. (1), as expected since the wall effectively becomes invisible in this limit. In contrast, for a hole with a resonant membrane, near-unity transmission is attained for zero M_{eff} [18].

The bare-hole lossless result $\tau = 1$ for $\alpha \to 0$ is not accurate, for example, when δ/r is not negligible ($\delta = 69$ μm at 1 kHz, so this means when $r \lesssim 0.5$ mm—see the Supplemental Material [49]), in which case losses dominate, or when α is too large ($\alpha > 0.1$) [29,40], in which case near-field hole interaction effects arise; Eq. (6) should then be used, but the general trends are similar. The interaction effect increases the transmittance except under conditions near $kr \to 0$, where the interaction does not affect the transmittance expressed in Eq. (6). Therefore, for a constant filling fraction α, the hole interaction effect mitigates the tendency for a decrease in transmittance when kr is increased.

The case of a single hole deserves discussion: for a hole in a deeply subwavelength diameter waveguide, the result is the same as for an array of holes in an infinite plate with a hole spacing $d \sim D$ equal to the waveguide diameter (see the Supplemental Material). In contrast, for a single hole in an infinite, thin plate, the transmission efficiency is $\eta = 8/\pi^2 \approx 0.81$ in the limit $r \ll \lambda$ without losses [4,5,27]. In a deeply subwavelength diameter waveguide, efficient transmission with $\eta \equiv \tau/\alpha \approx 1/\alpha$ when $\tau \approx 1$ cannot therefore be explained by the linear superposition of the individual transmissions of each hole. Instead, the phenomenon owes its existence to far-field constructive interference arising from the holes acting as subwavelength-spaced sources in a plane.

III. EXPERIMENTAL RESULTS AND COMPARISON TO THEORY AND SIMULATIONS

A. Experimental method

For experimental investigation, we use an acrylic waveguide of inner diameter $D = 100$ mm, thickness 5 mm, and length 2.3 m, shown in Fig. 1(a), and 15 perforated aluminium plates of thickness 1 mm, shown in Fig. 1(b), all with the same filling fraction $\alpha = 0.123$. N, shown in order, corresponds to holes of diameter 35.0, 24.8, 20.2, 17.5, 15.7, 14.3, 13.2, 12.4, 11.7, 11.1, 10.55, 9.05, 7.8, 5.0, and 3.5 mm (±0.1 mm). The plates are clamped between two sections of tube with modeling clay, as explained in the Supplemental Material [49].

Single-tone 1.0 kHz sound ($\lambda = 0.343$ m, $D = 0.29\lambda$, $r \ll \lambda$) is sent from a loudspeaker at one end of the tube at normal acoustic incidence, using anechoic termination with microperforated paper at the other end, showing a power reflection coefficient of ∼1%. τ and Γ are measured by obtaining the SWR (standing wave ratio) with the use of probe microphones [37]. Since $D \ll \lambda$, only waves with plane wave fronts travel down the tube. We ignore the effect of lateral or longitudinal resonances associated with the hole arrays and

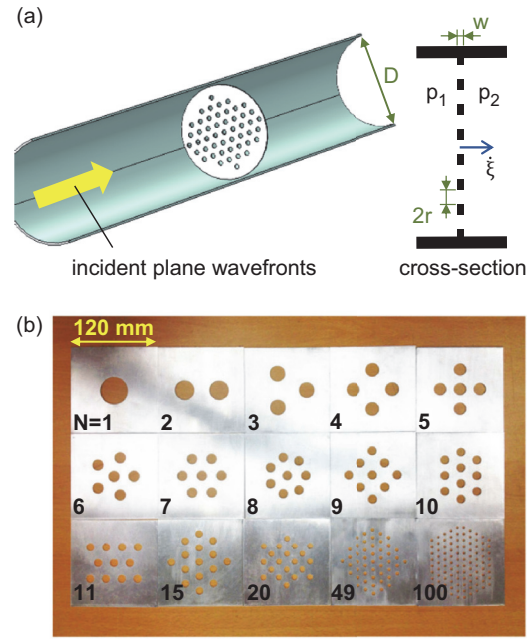

FIG. 1. (a) Schematic of the experimental geometry. Inset: cross-sectional view of the perforated wall. The loudspeaker and anechoic termination are not shown. (b) Image of the set of aluminium plates used for mounting in the $D = 100$ mm inner-diameter acrylic circular waveguide. The number of holes N in each plate is indicated.

the hole length w, respectively, owing to $\lambda \gg w$ and $\lambda \gg d$ [12].

B. Experimental results for transmission and comparison to theory and simulation

The experimental τ and Γ are plotted vs kr as dots in Figs. 2(a) and 2(b), respectively. As expected, τ increases and Γ decreases on decreasing kr. Strikingly, τ reaches a value of 0.88 for the smallest value of $r = 1.75$ mm ($kr = 0.032$), which corresponds to $N = 100$, even though only ∼12% of the tube is open. We also plot in Fig. 2 with a blue solid line the predictions of Eqs. (6) and (7), using literature values of the relevant physical parameters of air at 20 °C and 1 atm: $\rho_0 = 1.20$ kg/m^3, $c_0 = 343$ m/s, and $\mu = 1.81 \times 10^{-5}$ kg/m · s [41]. Although Eqs. (6) and (7) are within their range of validity for all the perforated plates at 1 kHz, there is some deviation between the predictions and experiment, particularly at high kr. Structural vibration of the plates is probably responsible for this (see the Supplemental Material [49]). We predict $\tau = 0.94$ for $r = 1.75$ mm, close to the experimental value. The predicted τ shows a maximum at $\tau = 0.95$ near $kr = 0.014$ ($r = 0.77$ mm $\sim w$), owing to the increase in viscous damping on decreasing r. As previously discussed, for low inertance I_{eff}, which implies near-unity transmission—for example $\tau > 0.95$—we require $(kw/\alpha)(1 + 2\Delta w/w) < 0.5$ [from Eq. (6) for no losses]. At 1 kHz, where $kw/\alpha = 0.15$, this condition is satisfied for $N = 49$ and 100. Neglecting losses but including hole interactions (dotted lines) gives poorer agreement, as expected. Plots that also neglect near-field hole interactions, i.e., according to Eq. (8), are given in the Supplemental Material [49]. The detailed arrangement of the holes in the plates is not expected

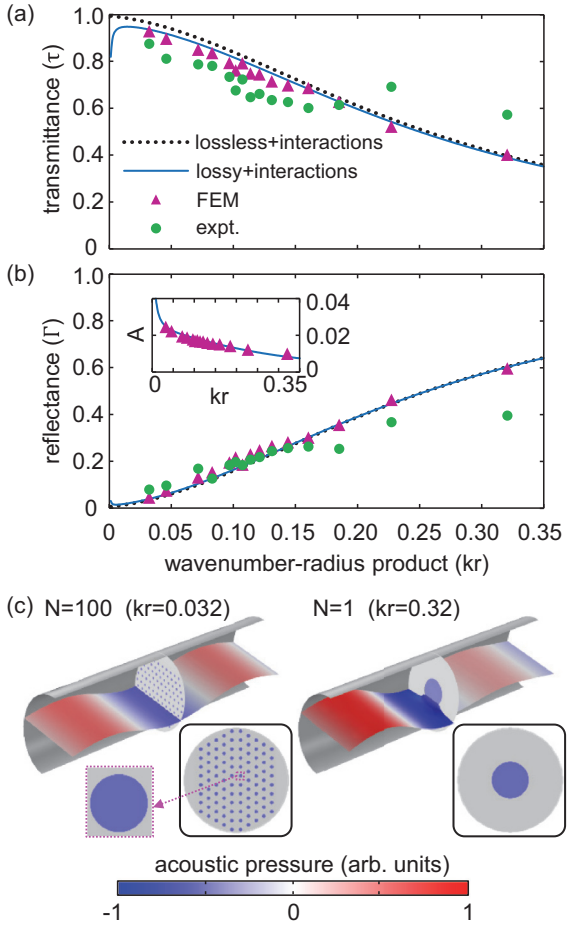

FIG. 2. (a) and (b) Transmittance τ and reflectance Γ vs wavenumber-radius product kr of perforated walls for $kw = 0.018$ at 1.0 kHz and constant filling fraction $\alpha = 0.123$: experimental data (green dots), theory including losses and interactions between holes (blue solid line), FEM (purple triangles), and lossless theory (black dotted line). Inset: absorption coefficient A from theory including losses and interactions, compared with FEM. (c) 3D and cross-sectional views of the acoustic pressure field for $N = 1$ and 100. The cross-sectional views apply to planes bisecting the holes. The pressure map for $N = 100$ includes a zoomed-in view to show the uniform pressure distribution. See animations.

to significantly affect the transmission [29], but nonuniformity in the spatial distribution of the holes may cause residual deviations from the theory (see the Supplemental Material [49]).

To verify the theoretical approach for τ and Γ, we carried out finite-element simulations (FEM) using COMSOL multiphysics, including losses and assuming rigid solids. (Thermal losses are negligible compared to viscous losses; see the Supplemental Material [49]) τ and Γ from FEM are shown by the purple triangles in Figs. 2(a) and 2(b), respectively. The agreement with the theory including losses is very good. The absorption coefficient A from FEM is shown in the inset of Fig. 2(b), which is in accord with the theory based on $A = 1 - (\tau + \Gamma)$. Experimental results for A give larger values $\sim$0.1, owing, we believe, to structural damping by the clay, which can also contribute to a decrease in the observed τ.

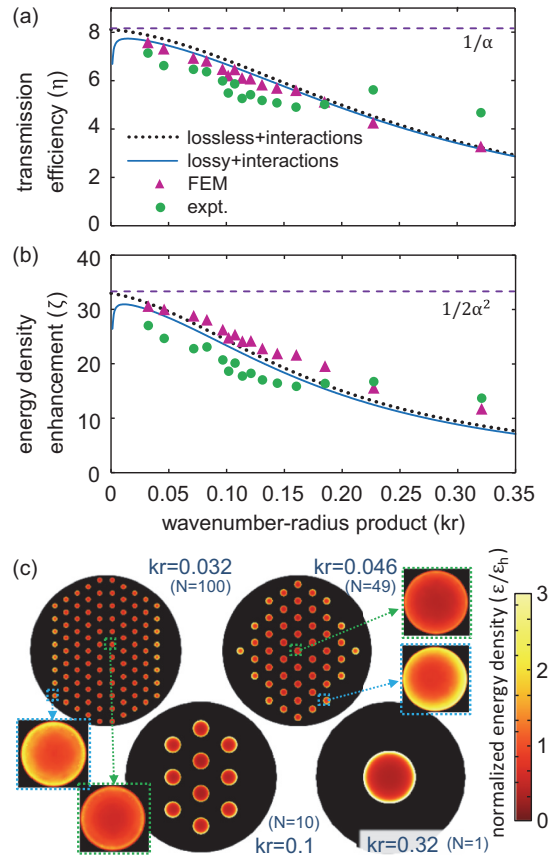

FIG. 3. (a), (b) Transmission efficiency η and acoustic energy density enhancement factor ζ vs wavenumber-radius product kr for $kw = 0.018$ at 1.0 kHz and constant filling fraction $\alpha = 0.123$, with the coloring scheme of Figs. 2(a) and 2(b). The dashed lines in (a) and (b) are the $\tau = 1$ values $\eta = 1/\alpha = 8.16$ and $1/2\alpha^2 = 33.3$. (c) Normalized energy density maps for different plates, plotted over the central bisecting plane of the plates. Insets: maps over individual holes, including zoomed-in views of central and peripheral holes when $N = 49$ and 100. See animations.

Figure 2(c) shows the simulated acoustic pressure fields on two planes parallel and perpendicular to the waveguide axis (at the central position) for $N = 1$ and 100. The front-view maps indicate that there is a uniform acoustic pressure field distribution inside the holes, as assumed in the analytical model.

C. Comparison of results for transmission efficiency with theory and simulations

The transmission efficiency $\eta = \tau/\alpha$ can be calculated from Eq. (6) as follows:

$$\eta = \frac{1}{\alpha(1+\chi^2)}\left(1 - 2\frac{\delta}{r}\frac{w''}{w'}\frac{(1+\chi)\chi}{1+\chi^2}\right). \tag{10}$$

Interestingly, all the plates used fall in the extraordinary-transmission category, as shown by the plot of η vs kr in Fig. 3(a) for the same four cases as in Figs. 2(a) and 2(b). The experimental η increases with decreasing kr, reaching $\eta = 7.2$ at $r = 1.75$ mm and $N = 100$, compared to $\eta = 7.6$ from the theory including losses and hole interactions. To emphasize the broadband nature of the transmission, we

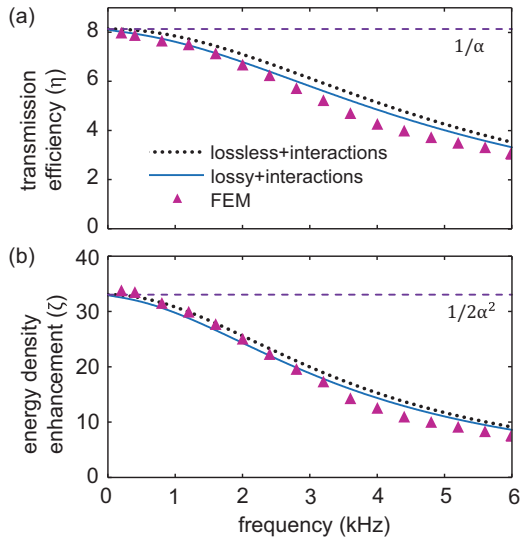

FIG. 4. (a), (b) Predicted and simulated transmission efficiency η and acoustic energy density enhancement factor ζ vs frequency f for $r = 1.75$ mm, $N = 100$, and constant filling fraction $\alpha = 0.123$, with the coloring scheme of Figs. 2(a), and 2(b).

plot in Fig. 4(a) the FEM and analytically calculated η as a function of f for the case of $r = 1.75$ mm and $N = 100$, both showing a broadband response with a FWHM (full width at half maximum) transmission bandwidth ∼5 kHz. This broadband behavior is in stark contrast to the case of a resonant metasurface [18]. The difference between analytical predictions and those of FEM increases as the frequency increases because of the assumption $kr \ll 1$ for the former.

Clearly there is nothing particularly "extraordinary" about this nonresonant $\eta > 1$. Consider Eq. (10) for the lossless case, which gives reasonable predictions. The inequality $\eta > 1$ can then be recast as a condition on the acoustic wavelength:

$$\lambda > \lambda_c \equiv \frac{\pi w}{\sqrt{\alpha(1-\alpha)}}\left(1 + \frac{16}{3\pi}\psi(\sqrt{\alpha})\frac{r}{w}\right), \qquad (11)$$

where λ_c, which decreases as r decreases, is the onset wavelength for extraordinary transmission. This emphasizes that longer wavelengths are conducive to larger η. For $r = 17.5$ mm, $\lambda_c = 0.158$ m from Eq. (11). Therefore, $\eta > 1$ for all the chosen values of r with $\lambda = 0.343$ m, as in the experiment. The blue solid curve in Fig. 3(a) shows that for small kr, owing to losses, η decreases below a maximum of 7.7 at $kr = 0.014$, which is itself below the $\tau = 1$ value $\eta = 1/\alpha = 8.16$ (the horizontal dashed line in the figure). In contrast, in optics for the case of an array of apertures in a thin perfect electric conductor, $\eta \sim \alpha r^2/\lambda^2 \to 0$ in the limit of deeply subwavelength hole separations [42]. Acoustic waves, unlike their electromagnetic counterparts, are not strongly evanescent inside subwavelength holes.

D. Comparison of results for energy concentration with theory and simulations

Extraordinary transmission through small holes implies sound concentration, with possibilities in high-performance acoustic energy harvesting [43,44]. By the conservation of energy, the average acoustic flux density is enhanced by a factor η in the holes. For applications, it is important to also calculate the acoustic energy density enhancement factor, $\zeta = \epsilon_h/\epsilon_1$, where ϵ_h and ϵ_1 are the spatiotemporally averaged energy densities inside the holes and before the perforated wall, respectively. Using a more precise theory for α, kr, $\delta/r \ll 1$ (see the Supplemental Material [49]),

$$\zeta = \frac{\tau}{2\alpha^2(1+\Gamma)} \approx \frac{1}{2\alpha^2}, \qquad (12)$$

where the approximation is for the case $\tau \approx 1$ (in which case $\Gamma \approx 0$). In our geometry, $1/(2\alpha^2) = 33.3$.

ζ vs kr is shown in Fig. 3(b) for the same four cases, with predictions from Eqs. (6), (7), and (12). The maximum ζ for the theory including losses is 30.9 at $kr = 0.0117$, whereas from the experiment using Eq. (12) and from theory including losses, we obtain 27.0 and 30.0, respectively, for $N = 100$ ($kr = 0.032$). This energy densification is significant in that no resonances are involved.

Maps of the FEM energy density, normalized to the analytically calculated value of ϵ_h, for $N = 1$, 10, 45, and 100 are shown in Fig. 3(c). The energy density ϵ ($= \mathrm{Re}[p]^2/2\rho_0 c_0^2 + \mathrm{Re}[u]^2\rho_0/2$) inside the holes tends to increase with the radial coordinate, reaching a maximum near the hole edges, and with proximity to the waveguide wall; spatial variations in the particle velocity u are responsible, irrespective of the essentially uniform acoustic pressure distribution. In general, the acoustic particle velocity reaches a maximum near the edge of a hole before dropping to zero at the boundary, an effect previously predicted and noted in holes with various geometries [45–47], and the average particle velocity for the outermost holes in the waveguide is higher than that for the central holes (see the Supplemental Material for the details of acoustic-field distributions [49]). That is, more air is funneled to the circumferential regions of a single hole, and, likewise, more air is funneled from the space outside the hole pattern regions to the outer holes. From the above-mentioned expression for ϵ and considering the quasiuniform pressure distributions, the spatial distributions of the acoustic energy density across the hole cross sections follow a similar trend to those of the corresponding particle-velocity distributions. These effects explain the residual differences between the analytical predictions and the FEM results (see the Supplemental Material [49] and animations). As in the case of η, the frequency-domain behavior of ζ, shown in Fig. 4(b) for the case of $r = 1.75$ mm and $N = 100$, shows a broadband response with a FWHM transmission bandwidth ∼3 kHz.

IV. CONDITIONS FOR OPTIMAL TRANSMISSION EFFICIENCY

The maximum η for a given w and k can be analytically calculated from Eq. (10) under the condition $\alpha \to 0$ ($\psi = 1$), using the approximation $w''/w' \approx 1$ (see the Supplemental Material for all the details [49]). In the lossless case, the transmission efficiency has an extremum for $\chi = 1$, giving optimal $\alpha = kw'/2$ when $\tau = 0.5$, which implies optimal $\eta = 1/(2\alpha)$ in the limit of small r. At 1 kHz and $w = 1$ mm as in our experiment, one obtains the optimal value $\eta = 55$ when

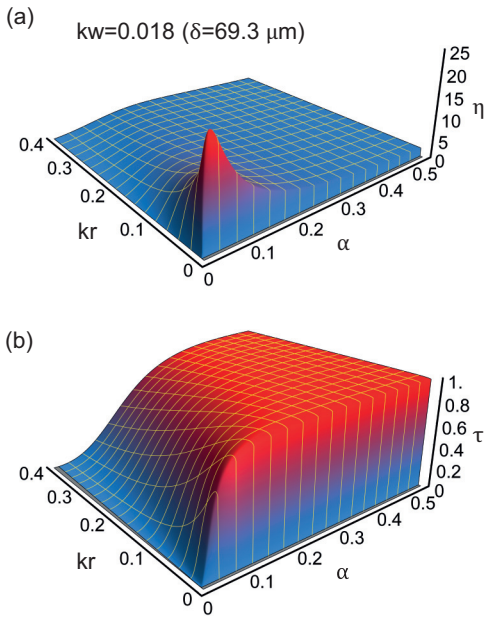

FIG. 5. (a), (b) Three-dimensional plots of the analytically calculated transmission efficiency η and transmittance τ vs filling fraction α and wavenumber-radius product kr for $kw = 0.018$ and viscous skin depth $\delta = 69.3$ μm, appropriate for air at room temperature with $f = 1$ kHz, including hole interactions.

$\alpha = 0.0092$ and $r/w \to 0$; losses reduce the optimal η to a value of 23 for $\alpha = 0.021$, $r/w = 0.45$, and $\tau = 0.47$. The transmission efficiency η from Eq. (10) without approximation and the transmittance τ from Eq. (6) are plotted as a function of kr and α as three-dimensional graphs in Figs. 5(a) and 5(b), respectively, for the case of $f = 1$ kHz. In contrast to the condition of low inertance leading to maximum $\tau \approx 1$, to obtain optimal $\eta = \tau/\alpha$ one requires $\tau \approx 0.5$ owing to the competing terms τ and α.

V. CONCLUSIONS

In conclusion, we have investigated optimal acoustic transmission τ through perforated plates. We measure τ for differing hole number N at constant filling fraction and plate thickness, for deeply subwavelength hole radius, spacing, and thickness. A metamaterial-based model including losses and hole interactions—a leading-order approximation of an acoustic theory based on far-field waves and boundary conditions that account for viscous losses and interactions between holes—has been developed, and is backed up by numerical simulations.

For large N we show that a hole array can act as a low-inertance metamaterial without resonance, thus explaining the near-unity transmittance and a transmission efficiency $\eta \approx 7$ observed at 1 kHz for 100 holes of diameter 3.5 mm with filling fraction $\alpha \approx 0.12$, and demonstrate that η is close to the optimum value as limited by viscosity and the chosen α. We also derive an acoustic energy density enhancement $\zeta \approx 27$, and find the value of and conditions for the maximum enhancement in transmission for a given wall thickness and frequency. This leads to the remarkable result that, without constraint on the filling fraction α, the condition for maximum transmission efficiency η corresponds to the case of ~50% acoustic power transmission.

This work does not diminish the efforts of researchers seeking to create acoustic extraordinary transmission by the use of local resonances, but instead serves to underline that it is not a narrow-band phenomenon restricted to resonant systems. We have also emphasized the differences to the optical case, for which nonresonant extraordinary transmission through holes is not encountered. It would be interesting to reproduce the geometries of this Letter for resonant membrane-covered holes in order to elucidate the trends there. And work remains to further optimize η and ζ by judicious choice of the hole geometry and shape, and to investigate applications to sound transparent screens, for example for use at bank service counters. Finally, and importantly, high energy acoustic densification opens the way to the use of bare holes in wideband energy harvesting, for example by the installation of induction coils and actuators in the holes [43].

ACKNOWLEDGMENTS

We acknowledge Grants-in-Aid for Scientific Research from the Ministry of Education, Culture, Sports, Science, and Technology (MEXT) as well as support from the Japanese Society for the Promotion of Science (JSPS). A. A. M. acknowledges support from the U.S. Department of Energy, Office of Basic Energy Sciences, under Award No. DESC0019126.

[1] H. A. Bethe, Phys. Rev. **66**, 163 (1944).
[2] C. Bouwkamp, Rep. Prog. Phys. **17**, 35 (1954).
[3] L. Rayleigh, *The Theory of Sound*, Vol. 2 (Dover, New York, 1945).
[4] E. Ritchie, J. Acoust. Soc. Am. **3**, 402 (1932).
[5] C. Bouwkamp, IEEE Trans. Antennas Propag. **18**, 152 (1970).
[6] C. Genet and T. W. Ebbesen, Nature (London) **445**, 39 (2007).
[7] T. W. Ebbesen, H. J. Lezec, H. Ghaemi, T. Thio, and P. A. Wolff, Nature (London) **391**, 667 (1998).
[8] F. G. De Abajo, Opt. Express **10**, 1475 (2002).
[9] M.-H. Lu, X.-K. Liu, L. Feng, J. Li, C.-P. Huang, Y.-F. Chen, Y.-Y. Zhu, S.-N. Zhu, and N.-B. Ming, Phys. Rev. Lett. **99**, 174301 (2007).
[10] B. Hou, J. Mei, M. Ke, W. Wen, Z. Liu, J. Shi, and P. Sheng, Phys. Rev. B **76**, 054303 (2007).
[11] B. Hou, J. Mei, M. Ke, Z. Liu, J. Shi, and W. Wen, J. Appl. Phys. **104**, 014909 (2008).
[12] J. Christensen, L. Martin-Moreno, and F. J. Garcia-Vidal, Phys. Rev. Lett. **101**, 014301 (2008).
[13] H. Estrada, F. J. Garcia de Abajo, P. Candelas, A. Uris, F. Belmar, and F. Meseguer, Phys. Rev. Lett. **102**, 144301 (2009).
[14] F. J. G. de Abajo, H. Estrada, and F. Meseguer, New J. Phys. **11**, 093013 (2009).
[15] J. Christensen, L. Martín-Moreno, and F. García-Vidal, Appl. Phys. Lett. **96**, 233505 (2010).

[16] Y. Zhou, M.-H. Lu, L. Feng, X. Ni, Y.-F. Chen, Y.-Y. Zhu, S.-N. Zhu, and N.-B. Ming, Phys. Rev. Lett. **104**, 164301 (2010).
[17] R. Fleury and A. Alù, Phys. Rev. Lett. **111**, 055501 (2013).
[18] J. J. Park, K. J. B. Lee, O. B. Wright, M. K. Jung, and S. H. Lee, Phys. Rev. Lett. **110**, 244302 (2013).
[19] M. Molerón, M. Serra-Garcia, and C. Daraio, Appl. Phys. Lett. **105**, 114109 (2014).
[20] B. C. Crow, J. M. Cullen, W. W. McKenzie, V. Koju, and W. M. Robertson, AIP Adv. **5**, 027114 (2015).
[21] J. Christensen, A. I. Fernandez-Dominguez, F. de Leon-Perez, L. Martin-Moreno, and F. J. Garcia-Vidal, Nat. Phys. **3**, 851 (2007).
[22] S. Mezil, K. Chonan, P. H. Otsuka, M. Tomoda, O. Matsuda, S. H. Lee, and O. B. Wright, Sci. Rep. **6**, 33380 (2016).
[23] T. Devaux, H. Tozawa, P. Otsuka, S. Mezil, M. Tomoda, O. Matsuda, E. Bok, S. Lee, and O. Wright, Sci. Adv. **6**, eaay8507 (2020).
[24] I. B. Crandall, *Theory of Vibrating Systems and Sound* (D. Van Nostrand Company, 1926), pp. 229–237.
[25] L. Sivian, J. Acoust. Soc. Am. **7**, 94 (1935).
[26] U. Ingard, J. Acoust. Soc. Am. **25**, 1037 (1953).
[27] K. Mulholland and H. Parbrook, J. Sound Vib. **5**, 499 (1967).
[28] T. H. Melling, J. Sound Vib. **29**, 1 (1973).
[29] V. Phong and D. Papamoschou, J. Acoust. Soc. Am. **134**, 1090 (2013).
[30] J.-Y. Qian, L. Wei, G.-R. Zhu, F.-Q. Chen, and Z.-J. Jin, Energy Convers. Manag. **109**, 86 (2016).
[31] M. Rettinger, SMPTE J. **91**, 1171 (1982).
[32] S. Fukuhara, S. Kageyama, Y. Tai, and K. Yoshida, J. Audio Eng. Soc. **42**, 1020 (1994).
[33] J. Allard and N. Atalla, *Propagation of Sound in Porous Media: Modelling Sound Absorbing Materials* (John Wiley & Sons, 2009).
[34] V. Fock, Proc. USSR Acad. Sci. **31**, 875 (1941).
[35] D. Homentcovschi and R. N. Miles, J. Acoust. Soc. Am. **131**, 1158 (2012).
[36] V. Naderyan, R. Raspet, C. J. Hickey, and M. Mohammadi, J. Acoust. Soc. Am. **146**, EL399 (2019).
[37] D. T. Blackstock, *Fundamentals of Physical Acoustics* (John Wiley & Sons, 2000).
[38] N. Atalla and F. Sgard, J. Sound Vib. **303**, 195 (2007).
[39] R. Tayong, T. Dupont, and P. Leclaire, Appl. Acoust. **72**, 777 (2011).
[40] V. S. Nesterov, Proc. USSR Acad. Sci. **31**, 879 (1941).
[41] Material Database in COMSOL MULTIPHYSICS 6.0.
[42] R. Gordon, Phys. Rev. A **76**, 053806 (2007).
[43] M. A. Pillai and E. Deenadayalan, Int. J. Precis. Eng. Manuf. **15**, 949 (2014).
[44] J. Choi, I. Jung, and C.-Y. Kang, Nano Energy **56**, 169 (2019).
[45] A. M. Davis and R. J. Nagem, J. Acoust. Soc. Am. **113**, 3080 (2003).
[46] S. Weyna, W. Mickiewicz, P. Michał, and M. Jabłoński, Arch. Acoust. **38**, 211 (2013).
[47] W. Chang, L. Yang, Z. Zhu, Z. Yang, Y. Hao, and C. Gao, Sensors **21**, 4337 (2021).
[48] Holes always intrinsically interact by acoustic interference in the far field.
[49] See Supplemental Material at http://link.aps.org/supplemental/10.1103/PhysRevB.108.144111 for details of (1) analytical model based on far-field acoustic waves for a general thickness perforated wall, (2) acoustic pressure and particle-velocity, (3) acoustic energy density in the holes, (4) optimizing the transmission efficiency, (5) effect on transmission of the sound-solid interaction, (6) details of the numerical simulations by FEM, and (7) details of the experiment.
[50] $\psi(y) = 1 - 1.4092y + 0.33818y^3 + 0.06793y^5 - 0.02287y^6 + 0.03015y^7 - 0.01641y^8 + 0.01729y^9 - 0.01248y^{10} + 0.01250y^{11} - 0.00985y^{12}$.